Available online at www.sciencedirect.com
ScienceDirect
Journal of Sound and Vibration 317 (2008) 781–799
JOURNAL OF SOUND AND VIBRATION
www.elsevier.com/locate/jsvi

Numerical evaluation of sound propagating over green roofs

T. Van Renterghem*, D. Botteldooren

Department of Information Technology, Ghent University, Sint-Pietersnieuwstraat 41, B-9000 Gent, Belgium

Received 21 November 2007; received in revised form 27 January 2008; accepted 17 March 2008
Handling Editor: C.L. Morfey
Available online 5 May 2008

Abstract

Sound propagation over intensive and extensive green roofs was numerically studied by using the finite-difference time-domain method. The Zwikker and Kosten model was used to simulate sound propagation in the substrate layer itself. The presence of a green roof is mainly interesting in a street canyon configuration, and fits well in the concept of quiet sides. Positive effects of green roofs, relative to fully rigid roofs, are mainly observed at the octave bands with centre frequencies 500 and 1000 Hz. The source type was shown to be unimportant when considering this particular parameter. There is a linear relationship between the fraction of the roof covered with green and the decrease in sound pressure level at the non-exposed canyon. The slopes increase with octave band centre frequency. The width–height ratio of the street canyon configuration has only a limited effect. For extensive green roofs, a pronounced attenuation peak is found when varying the layer thickness, leading to a maximum reduction of up to 10 dB, relative to an acoustically rigid roof, for the octave band of 1000 Hz. A good overall efficiency is observed near the maximum layer thickness (15–20 cm) for this type of green roof. For an intensive green roof with a substrate layer thickness exceeding 20 cm, which is common, positive effects are not influenced anymore by substrate thickness.

1. Introduction

Vegetated rooftops (green roofs) have become increasingly popular. In Germany, for example, it is estimated that about 10% of all flat roofs are green. In Flanders (in Belgium), most local governments subsidize the construction of a green roof to a large extent.

Green roofs can be categorised as extensive or intensive, depending mainly on the depth of the growing medium. Extensive green roofs need only a thin layer of soil substitute or substrate. They support low-growing plants that are extremely sun and drought tolerant, like Sedum species and grasses. Intensive green roofs (often called roof gardens) on the other hand require larger soil depths, and may contain shrubs or even trees, just as in conventional gardens. Due to its large weight, constructional issues may occur in the case of intensive green roofs, in contrast to extensive roof systems.

Vegetated rooftops have a large number of ecological and economic advantages. Most often cited is the increase in thermal insulation of roof systems, leading to a decrease in energy costs, in both hot and cold

*Corresponding author. Tel.: +32 9 264 99 94.
E-mail address: Timothy.Van.Renterghem@intec.Ugent.be (T. Van Renterghem).

0022-460X/$ - see front matter © 2008 Elsevier Ltd. All rights reserved.
doi:10.1016/j.jsv.2008.03.025

climates [1–3]. Green roofs may also store a large amount of water, thereby significantly reducing the runoff peak of rainfall events [4–6]. Since urban areas consist mainly of impervious surfaces, green roofs help to reduce flooding risks. Green roofs may contribute to an improved air quality—directly or indirectly—as well. Plant structures like leaves and branches filter airborne particles from the air. Indirectly, the temperature reduction in cities leads to a reduced production of atmospheric ozone [7]. Uncovered roofs are further subject to very large surface temperature fluctuations, inducing stresses on the roof system and materials. Vegetation and substrate moderate these temperature fluctuations [8], and act therefore as a protection for the roof membrane. It was shown in Ref. [9] that life cycle costs of extensive green roofs are lower than those of exposed flat roofs, even without considering potential energy savings. Other advantages are an increase in carbon dioxide uptake, an improved biodiversity in urban areas [10], and the creation of a more pleasant environment for citizens.

Research on the acoustical benefits of green roofs is rather scarce. Ref. [11] reports on measurements showing the large sound insulation capacity of vegetated roofs. Studies on sound propagation over vegetated rooftops have not been reported yet. Since the exterior of a non-vegetated roof is most often a rigid material, there is potential in reducing acoustic waves diffracting over houses and buildings. In this paper, it is numerically investigated to what extent a green roof decreases the sound pressure levels at the non-exposed side. Although houses are already efficient noise barriers, creating very quiet areas is useful. It was shown that inhabitants of noisy cities, with easy access to a quiet place, are generally less highly annoyed [12,13].

The centres of large cities consist of a number of confined spaces, enclosed by tall buildings. Therefore, the study of sound propagation between such ''city canyons'' is clearly relevant. Engineering models tend to overestimate the shielding in such geometries [14], indicating the need for wave-based models. Accurate sound propagation calculations between city canyons have been reported using the equivalent sources method [15] and the finite-difference time-domain method (FDTD) [16–18].

The current study focuses on the effect of green roofs, assuming a still atmosphere and flat façades. Detailed numerical calculations of sound propagation between city canyons with a coupled FDTD-PE (parabolic equation) method were reported in Ref. [17]. A parameter study was performed, and the effects of the width–height ratio of the canyons, façade absorption, diffuse reflection, the presence of balconies, and building-induced refraction of sound (in a turbulent and non-turbulent atmosphere) were quantified. In addition, combinations of parameters were studied, like downwind sound propagation in the presence of diffusely reflecting façades.

Due to computational limitations, the numerical simulations in this paper are essentially two-dimensional. This means that a coherent line source is modelled. When expressing sound pressure levels relative to free field sound propagation, the coherent line source solution is equivalent to a point source solution [19]. A traffic flow, however, is more accurately described by an incoherent line source. The approach, as described in Refs. [17,20], enables constructing the incoherent line source solution based on a number of coherent line source simulations. The impact of the source type on the effect of the green roof will be studied as well.

The remainder of this paper is organised as follows. In Section 2, the numerical FDTD method is described together with the ground model, and their numerical parameters are discussed. Section 3 compares sound propagation calculations from a coherent and an incoherent line source for the particular situation of sound propagation between city canyons. Sections 4 and 5 present and discuss the numerical results of the green roof effect on waves diffracting over buildings. Finally, conclusions are drawn in Section 6.

2. Sound propagation model and parameters

Sound propagation from a ''source canyon'' towards a ''receiver canyon'' is studied, as shown in Fig. 1. The origin is located at the left bottom of the source canyon. Both canyons have a width W_c, and the central building has a width W_b. All buildings have an equal height H. The green roof is located on top of the central building. Parameter D indicates the distance between the edges of the building and the beginning of the green part of the roof. Parameter S indicates the depth of the green roof soil or substrate. Multiple layers may be present. All horizontal planes are acoustically rigid, except for the green part of the roof. The façades of the buildings are fully specularly reflecting (flat) and partly absorbing.

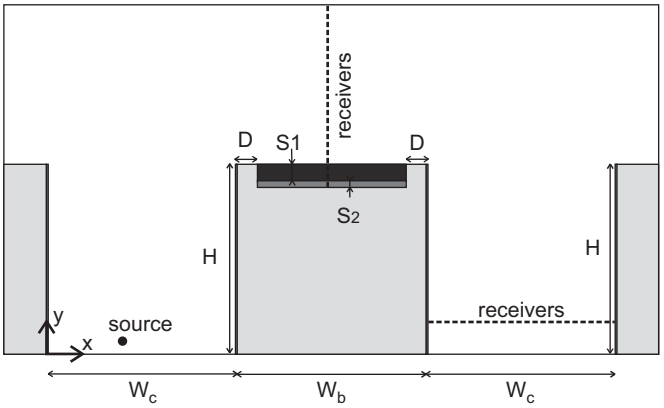

Fig. 1. Sound propagation configuration under study. The origin is located at the left bottom of the source canyon. The geometrical parameters W_c, W_b, H, and D are indicated. The substrate layer on top of the central building is shown, together with the soil depth S. A horizontal line of receivers is present in the receiving canyon, and a vertical receiver line above the central building.

The sound propagation equations in a still and homogeneous medium are given by

$$\nabla \cdot p + \rho_0 \frac{\partial \mathbf{v}}{\partial t} = \mathbf{0}, \tag{1}$$

$$\frac{\partial p}{\partial t} + \rho_0 c_0^2 \nabla \cdot \mathbf{v} = 0. \tag{2}$$

In these equations, p is the acoustic pressure, $\mathbf{v}$ is the particle velocity, ρ_0 is the mass density of air, c_0 is the adiabatic sound speed, and t denotes time. Viscosity, thermal conductivity, molecular relaxation, and gravity are neglected.

The FDTD method is used to solve the wave equations (1) and (2). A staggered spatial grid and a staggered time discretisation are applied [21]. Staggered-in-space means that the acoustical variables (pressure and the components of the particle velocity) are not discretised at the same physical locations in the computational grid. Staggered-in-time means that the pressure and velocity fields are not updated at the same, discrete times. An overview of the discretised FDTD equations used in this study can be found in Appendix A. The central difference approximation of the spatial and temporal derivatives in such a scheme results in second-order accuracy [21]. The stencil is very limited, which makes the implementation of boundary conditions and interfaces between different propagation mediums simple. On material boundaries, only particle velocities appear. Sound reflection from the façades is modelled using the impedance plane approach, as described in Ref. [21]. The normalised real-valued frequency-independent surface impedances of the façades equal 10. Perfectly matched layers are applied at the left and right boundaries (above the buildings), as well as at the upper boundary of the FDTD computational domain, to simulate an unbounded atmosphere.

Numerical stability is ensured as long as the Courant number is smaller than or equal to 1 [21]. The numerical model is free of amplitude errors [21]. The phase error is smallest when propagating along the diagonal of the computational cells and if the Courant number equals 1 [21].

Sound propagation inside the soil is described by means of the phenomenological porous-rigid frame model of Zwikker and Kosten [22]:

$$\nabla \cdot p + \rho' \frac{\partial \mathbf{v}}{\partial t} + R\mathbf{v} = \mathbf{0}, \tag{3}$$

$$\frac{\partial p}{\partial t} + \rho' c'^2 \nabla \cdot \mathbf{v} = 0, \tag{4}$$

$$\rho' = \frac{\rho_0 k_s}{\varphi}, \tag{5}$$

$$c' = \frac{c_0}{\sqrt{k_s}}. \tag{6}$$

Compared to Eqs. (1) and (2), a damping term is introduced based on the flow resistivity R of the ground medium. The mass density of the soil (i.e. an air and solid mixture) ρ' and the speed of sound in the ground c' are adapted using its porosity φ and structure factor k_s. The previous Eqs. (3)–(6) reduce to Eqs. (1) and (2) when $R = 0$, $\varphi = 1$ and $k_s = 1$. The discretised ground propagation equations can by found in Appendix A. It was shown in Ref. [23] that the above-described 3-parameter model can be used for accurate sound propagation modelling over finite-impedance ground.

The spatial discretisation scheme is illustrated in Fig. 2, showing the locations of the particle velocities and acoustic pressures near the edge of the building top. To perform time stepping, only direct neighbouring particle velocities or pressures are involved. The use of such a compact scheme allows an easy implementation, although different propagation mediums and different boundary types are situated very close to each other.

By including the ground in the propagation domain, in contrast to modelling sound reflection from an impedance plane [21,24], substrate depth may be varied as well. This allows discriminating more accurately between an extensive and intensive green roof.

It can be derived that the normalised acoustic impedance Z of an infinitely thick and homogeneous medium, obeying Eqs. (3)–(6), equals:

$$Z = \sqrt{\frac{R}{\rho\omega\varphi} j + \frac{k_s}{\varphi^2}}. \tag{7}$$

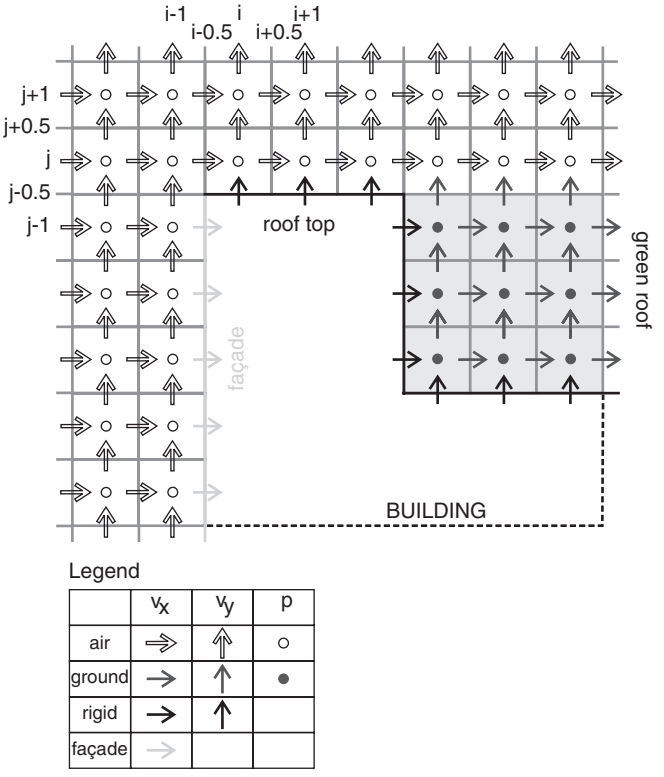

Fig. 2. Schematic representation of the locations of the particle velocities and acoustic pressures near the edge of the rooftop of the central building. The distinction is made between locations with different FDTD equations.

In Ref. [25], it was indicated that the accuracy of the Zwikker and Kosten model could be improved by making the ground parameters frequency dependent, especially when modelling attenuation by acoustically soft porous materials. The Zwikker and Kosten model, with frequency-dependent parameters, can be written in a form equivalent to the Wilson viscous/thermal relaxation model [26]. The time-domain implementation of the latter was discussed in Ref. [25]. It was shown however that memory-intensive evaluations of convolution integrals are needed, limiting practical applications.

The ground parameters used for the calculations in this paper are estimated from literature review. An intensive green roof constitutes typically of loose, uncompacted earth, above a drainage layer. A flow resistivity of 50 kPa s m^{-2} [27] is appropriate for the top layer. The porosity and structure factor of a soft soil are used [25]: $\varphi = 0.45$ and $k_s = 1.35$. For the drainage layer, measured values of gravel with a maximum particle size of 1 cm are used: $R = 5$ kPa s m^{-2} [28], $\varphi = 0.40$ [28], and $k_s = 1.5$ [25]. The extensive green roof substrate is usually a layer of granular material, like e.g. clay pellets [11]. The following values are used: $R = 10$ kPa s m^{-2}, $\varphi = 0.40$, and $k_s = 1.5$. For the porosity and structure factor, the values of gravel with a maximum particle size around 1 cm are used. The substrate thickness S of intensive roofs is typically between 20 and 60 cm. For extensive green roofs, values range from about 5 cm to 15–20 cm.

The presence of vegetation on the "green" roof is not considered in this study. Scattering on plant elements is mainly a high-frequency phenomenon. Since the sound propagation problem is governed by diffraction over a building, mainly low frequencies will reach the non-exposed side with sufficient amplitude. High frequencies, on the other hand, are already largely attenuated when propagating over the building. Therefore, the additional reduction by propagating through multiple layers of foliage, or the increase in sound pressure level by scattering into the non-exposed canyon is not relevant for the noise climate in the shielded region.

For accurate calculations in case of sound propagation in air, roughly 10 computational cells per wavelength are needed for the highest frequency of interest. Sound calculations in this configuration will be performed including the octave band of 1000 Hz. The highest frequency is 1405 Hz. Higher frequencies are well shielded and absorbed by the atmosphere and are therefore of less relevance for the quiet side. This would lead to a spatial discretisation step of 2.5 cm. At the interface between ground and air, a finer grid is however needed to accurately simulate reflection. With increasing surface impedance, smaller grid steps are needed to capture the strong decay of the sound pressure in the ground layer.

The grid resolution required to accurately model reflection on the ground was investigated numerically. A plane wave, normal incident on a few ground cells was simulated. Based on the incident and ground-reflected

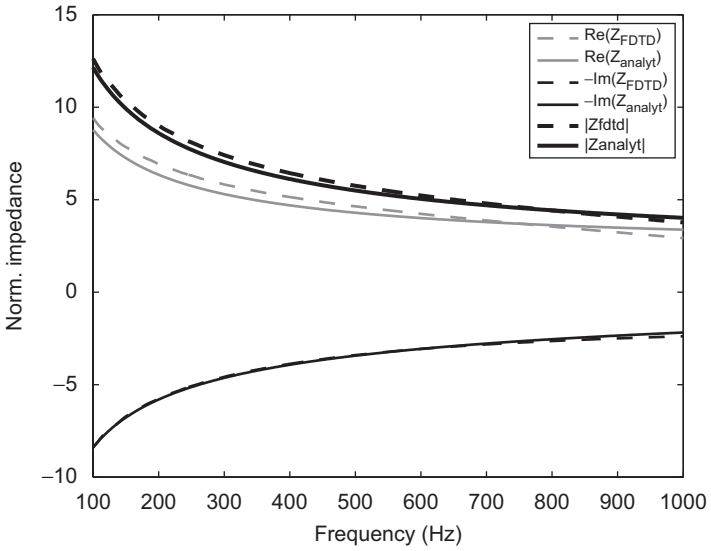

Fig. 3. Comparison between numerically obtained (dashed lines) and analytical (full lines) complex impedances. The real part (Re), imaginary part (Im), and the magnitude (| |) are considered. The following set of ground parameters is used: $R = 50$ kPa s m^{-2}, $\varphi = 0.45$, and $k_s = 1.35$. The spatial discretisation step is 1 cm, the Courant number equals 1.

pulse, the complex surface impedance of the soil was calculated. In Fig. 3, a comparison is made between the acoustic surface impedance obtained by the FDTD simulation with a 1-cm grid step, and the analytical impedance as described by Eq. (7). Since the plane wave is normal incident, the (characteristic) impedance of the ground medium equals its surface impedance. The real part, the imaginary part, and the magnitude of the normalised, complex impedance are considered separately. The ground parameters of loose earth were used in this analysis.

The use of a spatial discretisation step of 1 cm is shown to be sufficiently accurate. Such a discretisation leads to acceptable memory use and computing times when applied to the city canyon configuration. A grid refinement near the interface air-ground may however significantly decrease the computational cost. Care is however needed in such an approach. For accurate calculations, a gradual transition is needed to reduce spurious reflections in the refinement area [16]. When using a fixed time step, the Courant number in the coarse part of the computational domain will be much smaller than 1, leading to increased phase errors. Adapting the time-discretisation steps in each part of the computational domain on the other hand would further complicate the numerical implementation. For these reasons, such a grid refinement near the air–ground interface was not used.

For the simulations in this paper, the source is positioned at (4, 0.30). The vertical receiver line is placed in the centre of the middle building (15, y). Receiver points inside the substrate layer are included ($y<10$). The horizontal receiver line in the non-exposed canyon is placed at (x, 2), where x ranges from 20 to 30 m. The perfectly matched layers at the boundaries of the domain consisted of 40 computational cells, and absorption parameters were optimised. A broadband asymmetric Gaussian pulse is emitted at the source position.

The numerical parameters are as follows. The time-discretisation step equalled 20 μs, leading to a two-dimensional Courant number near one when using a spatial discretisation step of 1 cm. The simulation times were chosen to be long enough to capture all significant reflections in the canyons. After 30 000 time steps, sound pressure levels did not change anymore when $H = 10$ m and $W_c = W_b = 10$ m. At each time step, the pressure was recorded at the receivers, leading to a sampling frequency of 50 kHz. In all calculations, the sound speed in air c_0 is 340 m s^{-1}, and the mass density of air is 1.2 kg m^{-3}.

3. Influence of source type

Source type influences the shielding efficiency of noise barriers [29,30] and buildings [31]. In a street canyon configuration, a coherent line source causes strong destructive interferences, which are not observed when considering an incoherent line source. As a result, the shielding efficiency of a coherent line source is generally larger.

Ref. [29] shows how the sound pressure field from an incoherent line source may be calculated as a post-treatment of two-dimensional pressure fields. An important condition is that the sound propagation configuration has a constant cross-section: The geometry is unchanged by a translation in the z-direction. The calculation is based on a Fourier-type integration over a modified frequency spectrum. This method has been applied mainly to frequency domain techniques [29–32], leading to a large number of additional two-dimensional calculations over a wide range of frequencies. The application in an FDTD context has the advantage of only needing a single two-dimensional solution when working with a pulse-like source.

For accurately calculating point source solutions at very low frequencies (<100 Hz), or if finite-impedance materials are present, imaginary sound frequencies are needed. Unfortunately, such imaginary frequencies cannot be derived from a time-domain model. This means that the Fourier approach applied to the FDTD technique is limited to rigid surfaces only. The approach as described in Refs. [17,20] gives an alternative to calculating the incoherent line source solution based on coherent line source calculations. The incoherent line source in the street canyon is discretised in a number of point sources, as depicted in Fig. 4. For each point source, a calculation is performed in a vertical plane through the source and receiver. This approach uses the excess-attenuation equivalence between a coherent line source (point source in 2D) and a point source in 3D, as was theoretically derived in Ref. [19]. In the next step, the relative sound pressure levels from the different sources are averaged out energetically. This means that a 3D incoherent line source is modelled by performing a number of 2D simulations, with different canyon widths. In this approach, it is implicitly assumed that all buildings façades are oriented orthogonal to the different cross-sections where a calculation is made. Such a "twisting" of the façades is an approximation. This approach will be further indicated as "Twist".

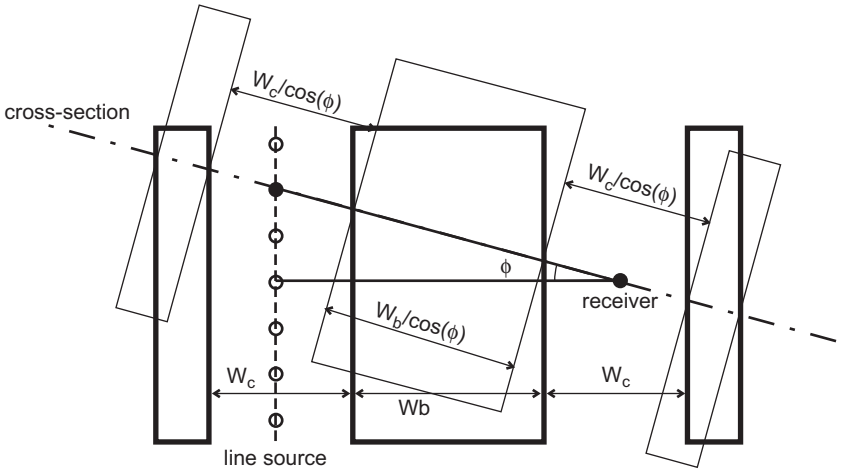

Fig. 4. Top view of the street canyon configuration, showing how an incoherent line source is modelled in two dimensions using the Twist approach.

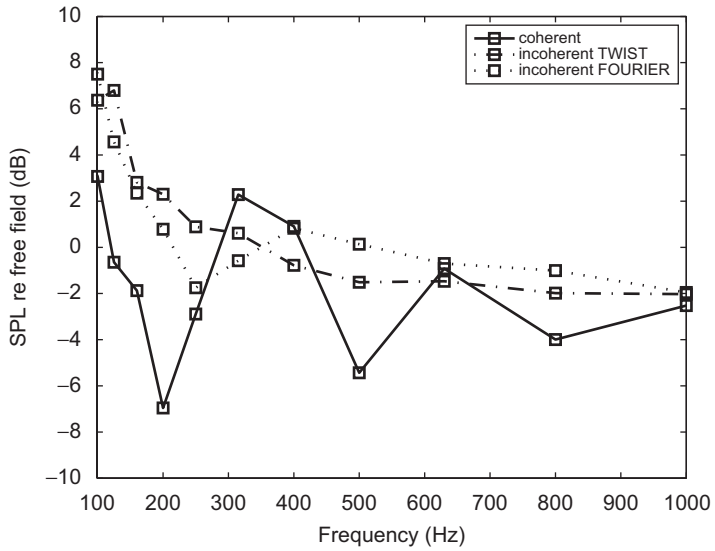

Fig. 5. Comparison between a coherent line source and an incoherent line source, as calculated by means of two approaches based on two-dimensional calculations (Twist, Fourier). The source is present at (2, 0.30), the receiver at (12.5, 2). The canyon height H, building width W_b, and canyon width W_c are all 5 m. All surfaces are rigid. Sound pressure levels are expressed in 1/3 octave bands and relative to free field sound propagation.

The Twist method is compared to the Fourier method in a numerical experiment. The comparison is possible for rigid surfaces only (see previous paragraphs). Under this condition, reverberation times in the canyons become very long. To keep computing times limited, the canyon widths W_c, the building width W_b, and the building height H were reduced to 5 m. The source was present at (2, 0.30), the receiver at (12.5, 2). The spatial discretisation step was 2 cm, the time step equalled 40 μs. The incoherent line source was represented by 17 equidistant point sources. Due to symmetry, sound propagation calculations for only 8 different canyon widths were necessary. The angle ϕ, as defined in Fig. 4, ranged from 0° to 70°. This corresponds to canyon widths ranging from 5 m to 17.22 m, respectively. Fig. 5 illustrates the good correspondence between the Fourier and Twist approach, expressed in 1/3 octave bands. Both approaches differ significantly from the coherent line source solution. The destructive interferences, especially at 200 and

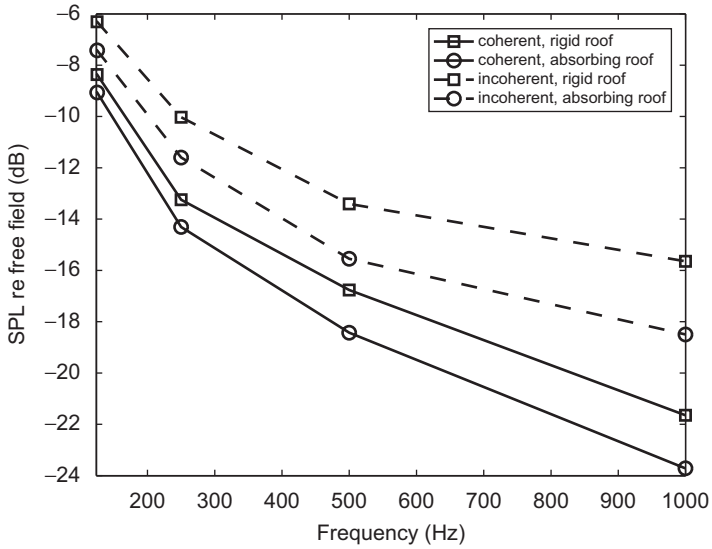

Fig. 6. Comparison between a coherent line source and an incoherent line source, as calculated by the Twist approach, in case of a fully rigid and absorbing roof ($D = 1$ m, $Z_0 = 10$). The façades are absorbing ($Z_0 = 10$). The source is present at (2, 0.30), the receiver at (12.5, 2). Sound pressure levels are expressed in octave bands, relative to free field sound propagation.

500 Hz, disappear in case of an incoherent line source. This comparison shows that the Twist approach is adequate to simulate an incoherent line source.

This paper will focus mainly on the effect of the presence of a green roof, relative to a rigid roof. It was therefore studied whether the time-consuming incoherent line source calculations need to be performed with the Twist approach for this specific quantity. To check this, a comparison was made between calculations for a rigid and absorbing roof (with a normalised real-valued surface impedance Z_0 equal to 10), using a coherent and an incoherent line source. The façades were partly absorbing as well ($Z_0 = 10$). Results are shown in Fig. 6. The sound pressure levels are expressed in octave bands, relative to free field sound propagation. The sound pressure levels caused by a coherent and incoherent line source are significantly different, but both are affected in a very similar way by introducing absorption on the roof. The difference in the effect is less than 0.7 dB. Therefore, it can be concluded that the green roof effect calculated using a coherent line source is valid for an incoherent line source as well.

4. Parameter study of an intensive green roof

In a first set of simulations, a two-layered intensive green roof is considered, constituting of a layer of gravel of 10 cm, below a layer of loose earth of 40 cm. The corresponding ground parameters of both layers can be found in Section 2. For comparison, numerical simulations for a fully rigid roof are performed in all situations.

The sound pressure levels for the octave bands with centre frequencies 125, 250, 500, and 1000 Hz are shown in Fig. 7, along the horizontal receiver line at $y = 2$ m in the non-exposed canyon. All sound pressure levels are expressed relative to free field sound propagation. In this simulation, the canyon widths W_c, the building width W_b, and building height H are all 10 m; D equals 1 m. In Fig. 8, the relative sound pressure levels are shown along the vertical array of receivers at $x = 15$ m, above the central building. The sound fields inside the substrate layers are shown as well.

At low frequencies, the acoustic impedance of a natural ground is high. As a consequence, the effect of the presence of the green roof, relative to a rigid roof, is limited for the octave bands of 125 and 250 Hz. At 500 and 1000 Hz, an important decrease in sound pressure level is observed in the non-exposed city canyon. For the octave band of 1000 Hz, the improvement compared to a rigid roof reaches 7 dB. Despite the presence of distinct zones with destructive and constructive interference, the effect of the green roof is quite uniform over the full length of the receiving canyon.

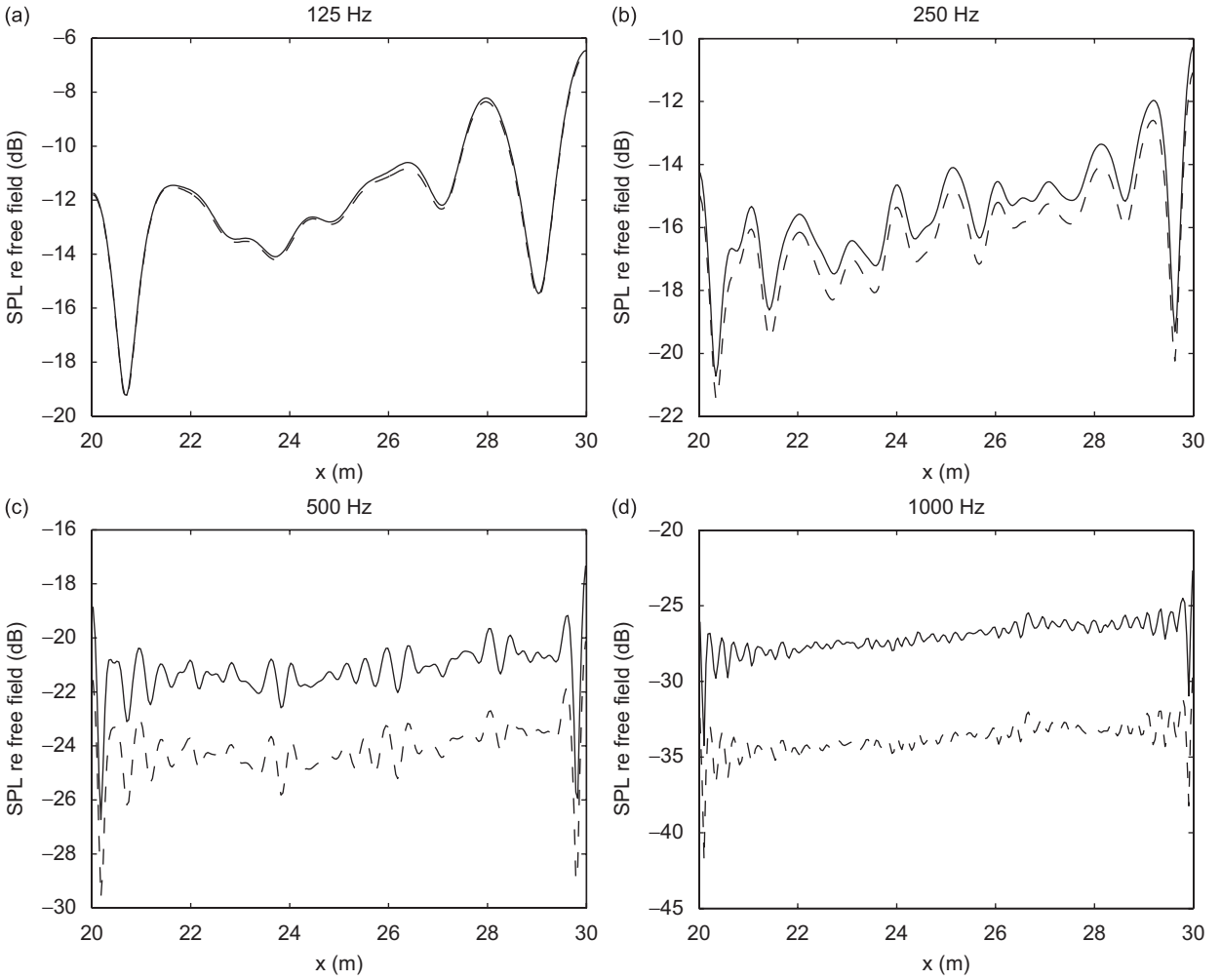

Fig. 7. Octave band sound pressure levels with centre frequencies 125 Hz (a), 250 Hz (b), 500 Hz (c), and 1000 Hz (d), relative to free field sound propagation, along the receiver canyon at $y = 2$ m. The full lines are for a fully rigid roof, the dashed lines for a two-layered intensive green roof ($S_1 = 40$ cm, loose earth; $S_2 = 10$ cm, gravel). ($W_b = W_c = H = 10$ m, $D = 1$ m, coherent line source).

It is further investigated whether the multiple reflections in the canyons affect the efficiency of placing a green roof. Therefore, a similar numerical experiment was performed, considering sound propagation over the central building only. This means that the canyon widths W_c went to infinity, and as a consequence, there was no street canyon configuration anymore. It is shown in Figs. 9 and 10 that in such a configuration, the effect of the green roof, relative to a rigid roof, is enhanced, especially at the octave bands with higher central frequencies. The additional reduction in sound pressure level at the octave bands of 500 and 1000 Hz, relative to a street canyon configuration, is between 2 and 3 dB. Close to the building, sound pressure levels are significantly smaller, since the diffraction angle is larger there. The sound pressure levels for a rigid roof however are already largely reduced compared to a street canyon configuration, because of the absence of multiple reflections. This means that the additional reduction by the presence of a green roof will not lead to a noticeable improved noise climate, since sound pressure levels are already very low. The positive effect of a green roof will therefore be observed mainly in a dense, urban environment.

The effect of the fraction of the roof surface covered with green is shown in Fig. 11. The influence of parameter D is studied, which is the distance between the edge of the building and the green part of the roof. A symmetrical design was chosen. The non-green parts of the roof were rigid in all simulations. The values of

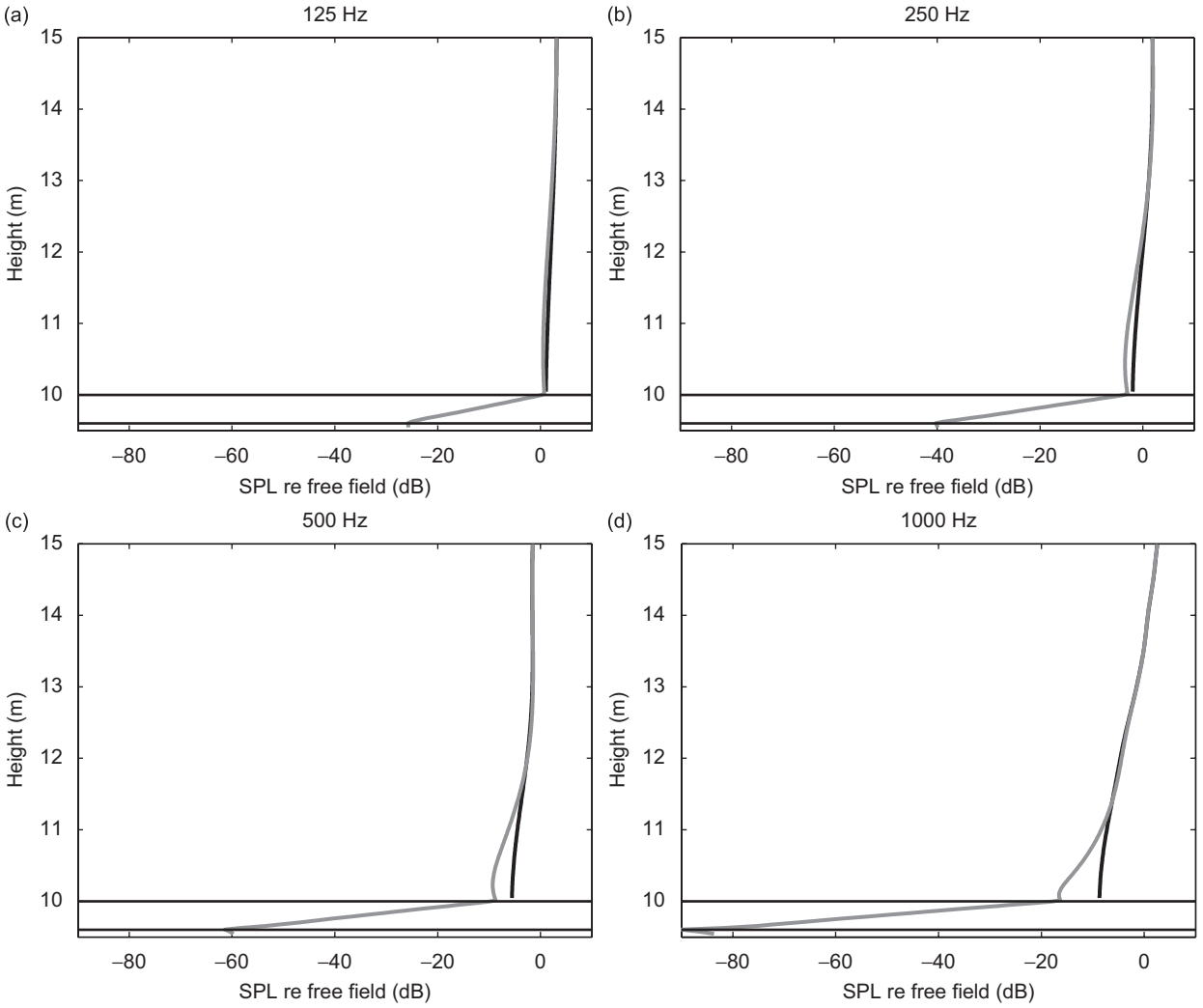

Fig. 8. Octave band sound pressure levels with centre frequencies 125 Hz (a), 250 Hz (b), 500 Hz (c), and 1000 Hz (d), relative to free field sound propagation, along a vertical line (at $x = 15$ m) above the central building. The black lines are for a fully rigid roof, the grey lines for a two-layered intensive green roof ($S_1 = 40$ cm, loose earth; $S_2 = 10$ cm, gravel). The sound pressure level distributions in the soil layer are shown as well ($W_b = W_c = H = 10$ m, $D = 1$ m, coherent line source).

D were 0.1, 1, 1.75, and 2.5 m, while the width of the central building W_c equalled 10 m. This corresponds to green roof fractions ranging from 98% to 50%. It is observed that with increasing D, the average effect of the green roof over the receiver line, relative to a complete rigid one, decreases. An almost perfectly linear relationship is found. The slope of this line increases with the centre frequency of the octave bands. The height of the receiver line does not influence this behaviour: Changing the receiver height ($y = 4$, 6, and 8 m) leads to very similar curves (not shown). This linear relationship indicates that the sound propagation problem is governed by diffracting waves, shearing over the building top. This is also illustrated by the vertical distribution of the sound pressure level, as shown in Fig. 8, for D equal to 1 m. Differences between the rigid roof and the partly green-covered roof appear only in the first metre above the roof. The presence of the layer of gravel is clearly observed in these figures as well. Because of the limited attenuation in the gravel layer, the reflection on the rigid roof, just below the gravel layer, becomes visible. The effect of the gravel layer, for sound propagating over the building, is negligible in this particular configuration. The error bars in Fig. 11 are the standard deviations of the effect of the green roof, relative to a rigid roof, over the line of receivers in the

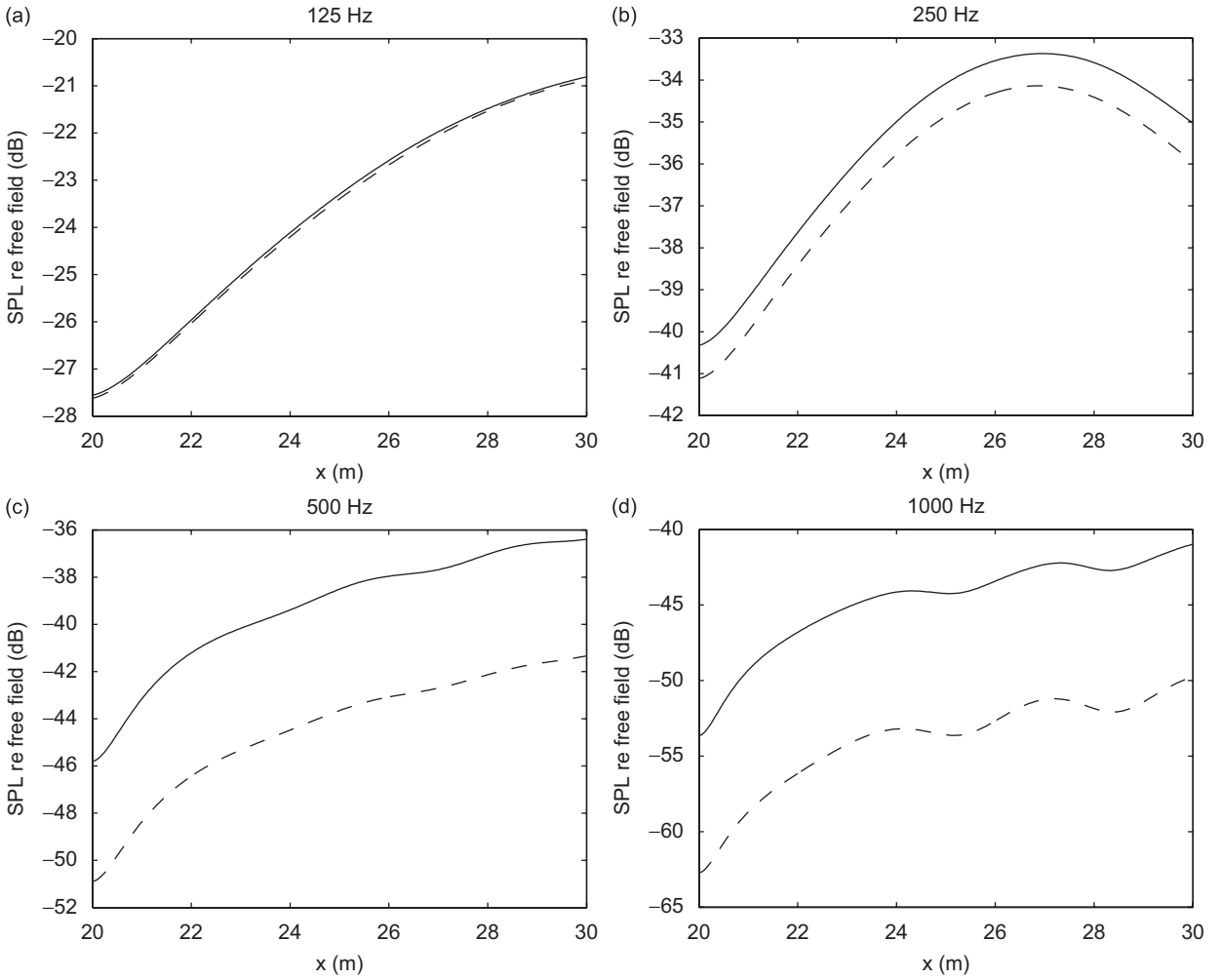

Fig. 9. Octave band sound pressure levels with centre frequencies 125 Hz (a), 250 Hz (b), 500 Hz (c), and 1000 Hz (d), relative to free field sound propagation, along the receiver canyon at $y = 2$ m. The full lines are for a fully rigid roof, the dashed lines for a two-layered intensive green roof ($S_1 = 40$ cm, loose earth; $S_2 = 10$ cm, gravel). ($W_b = H = 10$ m, $W_c =$ infinity, $D = 1$ m, coherent line source).

non-exposed canyon. These values are very small, indicating clearly that the studied effect is uniform over the receiver canyon.

The influence of the height of the buildings, forming the city canyons, is studied as well. The heights of the canyons H in the simulations were chosen to be 2.5, 5, 10, and 15 m. The canyon widths and the width of the central building were kept constant at 10 m. This leads to width/height ratios of 4, 2, 1, and 0.5, respectively. The source position remained unchanged. With increasing height, the reverberation times increased drastically. The simulation times were increased accordingly until the octave band results, at the receiver line at $y = 2$ m in the non-exposed canyon, did not change anymore. The average results over this line, together with their standard deviations, with increasing height of the buildings, are given in Fig. 12. The influence of the width/height ratio is very limited. Only at 1000 Hz, a slightly increased shielding (up to 1 dB) is observed by the presence of a green roof, relative to a rigid roof, when increasing the width/height ratio.

5. Influence of substrate layer thickness

In this section, the effect of layer thickness is studied for both an extensive and intensive green roof. Only homogeneous substrate layers were considered. In addition, numerical calculations were performed for

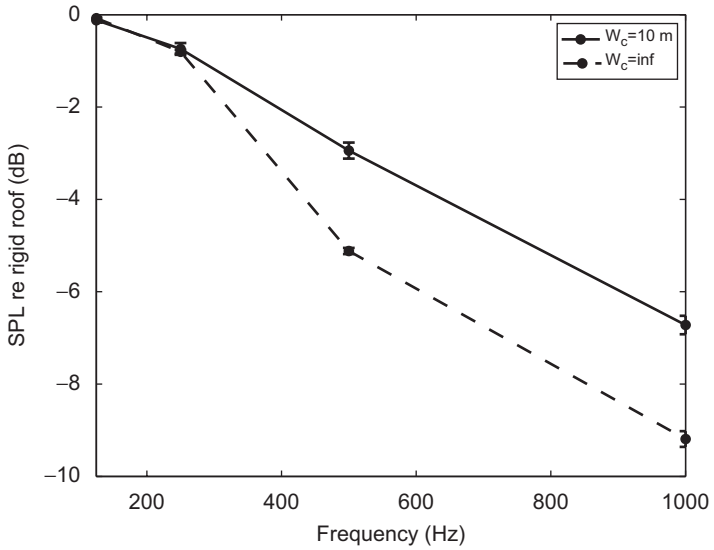

Fig. 10. Average effect with increasing frequency, along the receiver canyon at $y = 2$ m. Octave band sound pressure levels are shown relative to rigid roof octave band sound pressure levels. Both sound propagation in a street canyon configuration ($W_c = 10$ m) and in case of an isolated building ($W_c = \text{inf}$) are considered. The error bars show the standard deviations along the receiver line ($W_b = 10$ m, $D = 1$ m, $S_1 = 40$ cm, loose earth; $S_2 = 10$ cm, gravel).

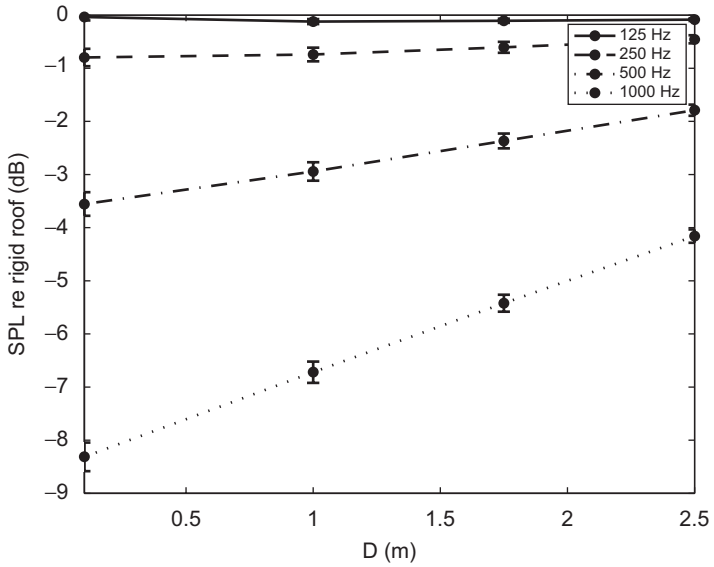

Fig. 11. Average effect of the distance between the building edge and the green part of the roof D, along the receiver canyon at $y = 2$ m. Octave band sound pressure levels are shown relative to rigid roof octave band sound pressure levels. The error bars show the standard deviations along the receiver line ($W_c = W_b = H = 10$ m, $S_1 = 40$ cm, loose earth; $S_2 = 10$ cm, gravel).

extensive green roofs exceeding their typical depths, and for intensive roofs with layer thicknesses that are much smaller than those observed in practice. This analysis indicates whether the typical substrate depths for both types, in combination with their ground characteristics, are optimal for sound diffracting over them. Layer thicknesses of 5, 10, 20, and 50 cm were simulated for both the extensive and intensive green roofs. The canyon widths W_c, the building width W_b, and building height H were all 10 m; D equalled 1 m.

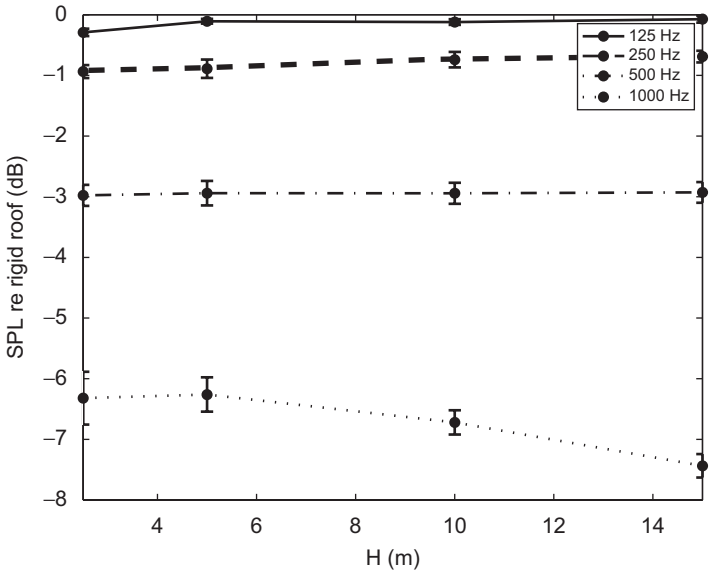

Fig. 12. Average effect of the canyon height H, along the receiver canyon at $y = 2$ m. Octave band sound pressure levels are shown relative to rigid roof octave band sound pressure levels. The error bars show the standard deviations along the receiver line ($W_c = W_b = 10$ m, $D = 1$ m, $S_1 = 40$ cm, loose earth; $S_2 = 10$ cm, gravel).

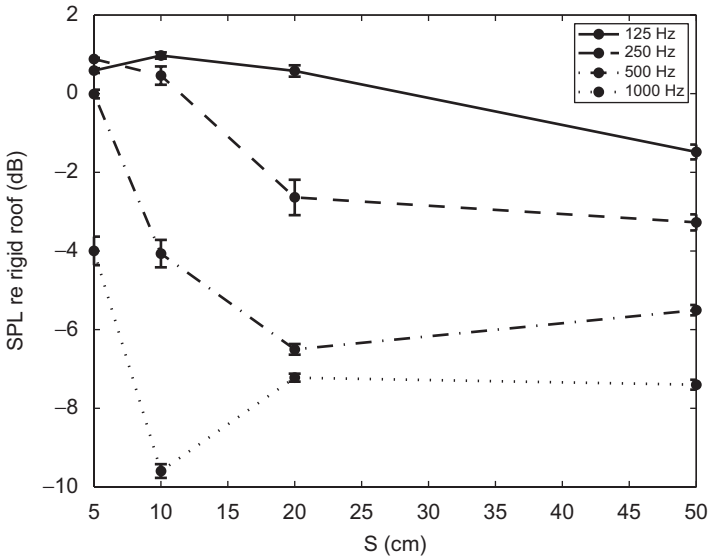

Fig. 13. Average effect of the substrate layer thickness S for an extensive green roof, along the receiver canyon at $y = 2$ m. Octave band sound pressure levels are shown relative to rigid roof octave band sound pressure levels. The error bars show the standard deviations along the receiver line ($W_c = W_b = H = 10$ m, $D = 1$ m, clay pellets).

Fig. 13 shows the influence of substrate (clay pellets) depth for the extensive green roof. The average decrease of the octave band sound pressure level, relative to a fully rigid roof, over the receiver line at a height of 2 m, is displayed. A 5-cm-layer gives an improvement for the 1000 Hz octave band only. At 125 and 250 Hz, a slightly worse situation, relative to a fully rigid roof, is observed for this thin substrate layer. The positive effect of the presence of a green roof starts from about 30 cm at 125 Hz, and from 15 cm at 250 Hz. An optimal layer thickness is observed, which shifts towards smaller values with increasing octave band centre frequency.

For the 500 and 1000 Hz octave bands, this minimum is found in the range of layer thicknesses that were simulated. For 1000 Hz, this optimum is near 10 cm, leading to a decrease of 10 dB compared to a fully rigid roof. At 500 Hz, this optimum is observed for a layer thickness near 20 cm, leading to 6 dB reduction. This minimum becomes more pronounced with increasing frequency.

In Fig. 14, the influence of substrate depth for an intensive green roof (loose earth) is shown. Sound pressure levels, relative to a rigid roof, are displayed, with increasing substrate layer thickness. Starting from about 20 cm, the effect of the green roof becomes nearly constant at all octave bands considered. For the octave band of 125 Hz, no improvement by the presence of a green roof is observed. For the 250 Hz octave band, the positive effect is smaller than 1 dB. For the octave bands of 500 and 1000 Hz, the improvement is important, and is respectively near 3 and 6 dB. The presence of a layer of gravel, as a drainage layer below the loose earth in the intensive green roof configuration (see Section 2), was not considered in this analysis. An intensive green roof typically consists of a substrate depth of at least 20 cm. It is clear from Fig. 14 that once a layer of loose earth of 20 cm is present, the substrate at larger depths does not influence anymore sound propagating over the building. Therefore, the gravel layer is not considered to be essential. Simulating a layer thickness below 20 cm has only limited practical applications. It illustrates nevertheless that the minimum, as observed in the case of an extensive green roof, is present here as well. It is shifted to lower substrate layer thicknesses, and these minimums are less pronounced compared to extensive green roofs. Additional simulations allowed determining more carefully the optimums. For the octave band with a centre frequency of 1000 Hz, it is observed at 6 cm. At 500 Hz, this optimum is found at 10 cm. For lower octave bands, this minimum is less pronounced.

Figs. 15 and 16 show in detail the sound pressure level distribution near the rooftop of the central building. The interaction between the incident (diffracting) wave and the sound wave propagating through the substrate and reflecting on the rigid roof just below the substrate layer results in a standing wave. For frequencies with a minimum sound pressure level in the receiving canyon, a node is found just above the rooftop. For a larger substrate thickness, this minimum is present inside the substrate. For a smaller layer, this minimum is present at some height above the rooftop. In case of the clay pellets layer, the phase of the substrate impedance is smaller than for the loose earth. This means that a larger substrate depth is needed to achieve a phase shift of π radials for sound waves travelling through the substrate and back. The optimum layer thickness of the extensive green roof for the 1000 Hz octave band is near 10 cm, while it is 6 cm for the intensive green roof.

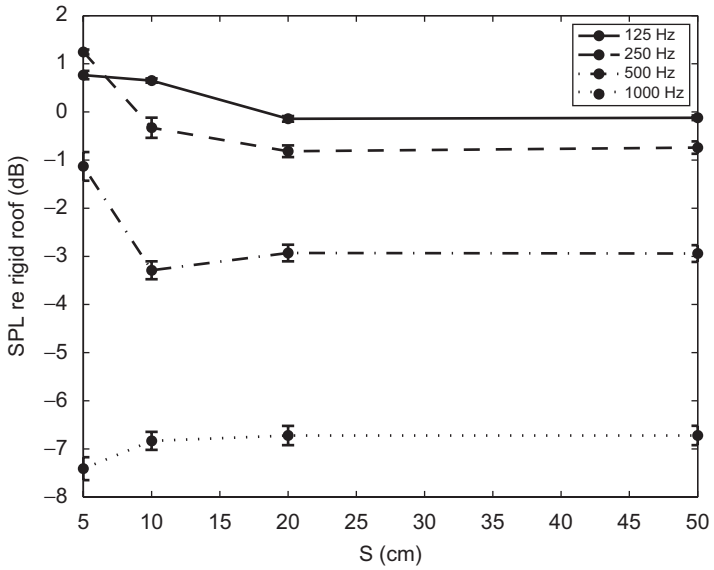

Fig. 14. Average effect of the substrate layer thickness S for an intensive green roof, along the receiver canyon at $y = 2$ m. Octave band sound pressure levels are shown relative to rigid roof octave band sound pressure levels. The error bars show the standard deviations along the receiver line ($W_c = W_b = H = 10$ m, $D = 1$ m, loose earth).

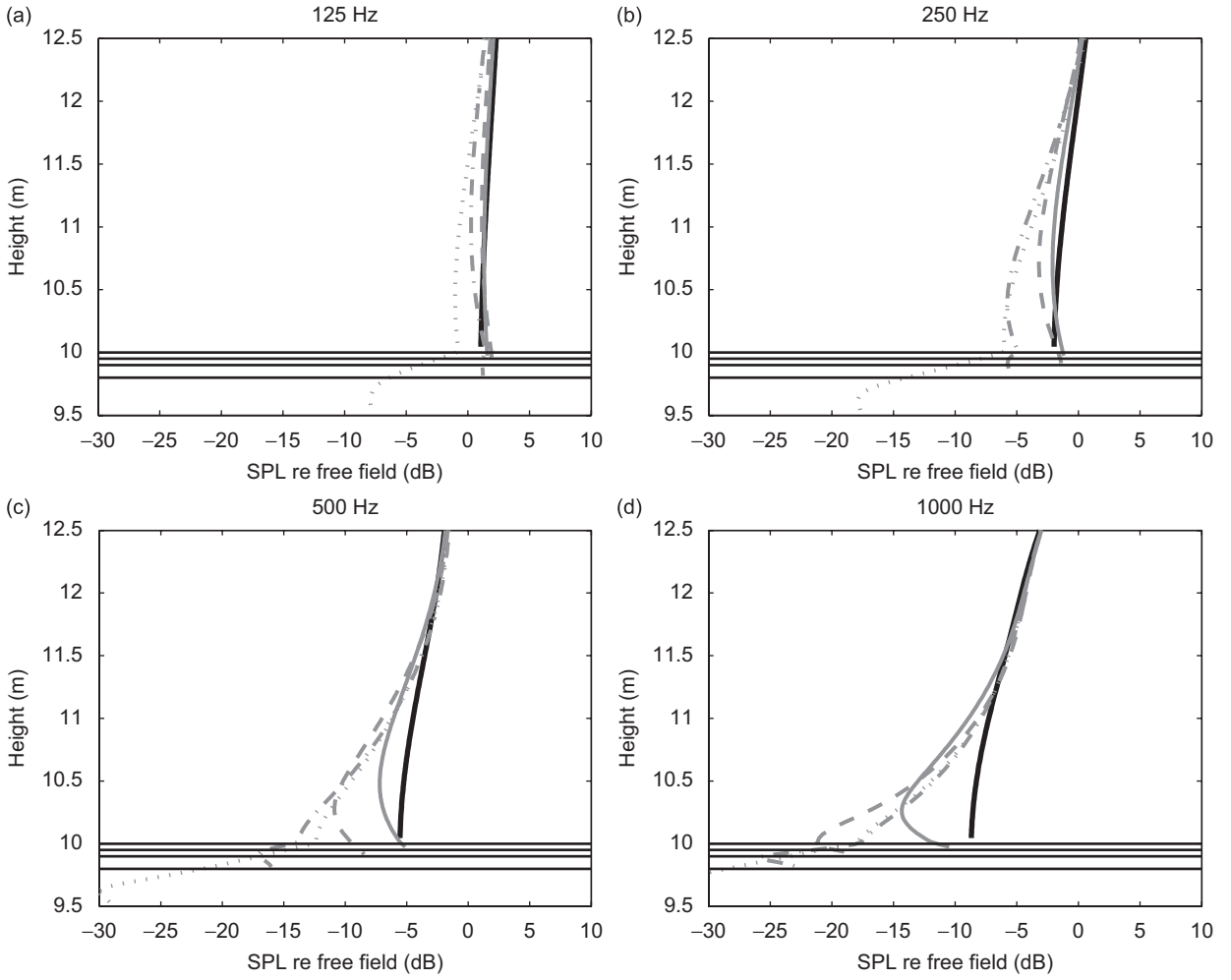

Fig. 15. Octave band sound pressure levels with centre frequencies 125 Hz (a), 250 Hz (b), 500 Hz (c), and 1000 Hz (d), relative to free field sound propagation, along a vertical line (at $x = 15$ m) above the central building. The full black lines are for a fully rigid roof. Extensive green roofs (clay pellets) with different substrate thickness are shown by the grey lines ($S = 5$ cm—full lines, 10 cm—dashed lines, 20 cm—dash-dotted lines, and 50 cm—dotted lines). The sound pressure level distributions in the soil layers are shown as well ($W_b = W_c = H = 10$ m, $D = 1$ m, coherent line source).

The maximum decrease in sound pressure level for the extensive green roof is larger, since the flow resistivity of the clay pellets is smaller. This means that the substrate-travelling wave will be less attenuated, and as a consequence, the destructive interference is stronger.

From this analysis, it can be concluded that both an extensive and an intensive green roof are interesting for reducing diffracting waves over a building. Even the small layer thicknesses of extensive green roofs may result in large attenuations. In the latter, the improvement is very sensitive to the layer thickness, especially for the octave band of 1000 Hz, where a distinct minimum is observed. A good overall efficiency is possible for a layer thickness near 15–20 cm. This is close to the maximum layer thickness of extensive green roofs. Since the substrate thickness of an intensive green roof usually exceeds 20 cm and the maximal acoustic effect is reached at this thickness, sound shielding is not increased anymore by thicker layers. When considering sound transmission through the roof system, however, large substrate depths may be interesting. For low frequencies, an extensive green roof slightly reduces the screening by the building but this negative effect is less than 1 dB. In case of an intensive green roof, no negative effect, relative to a fully rigid roof, is observed at low frequencies.

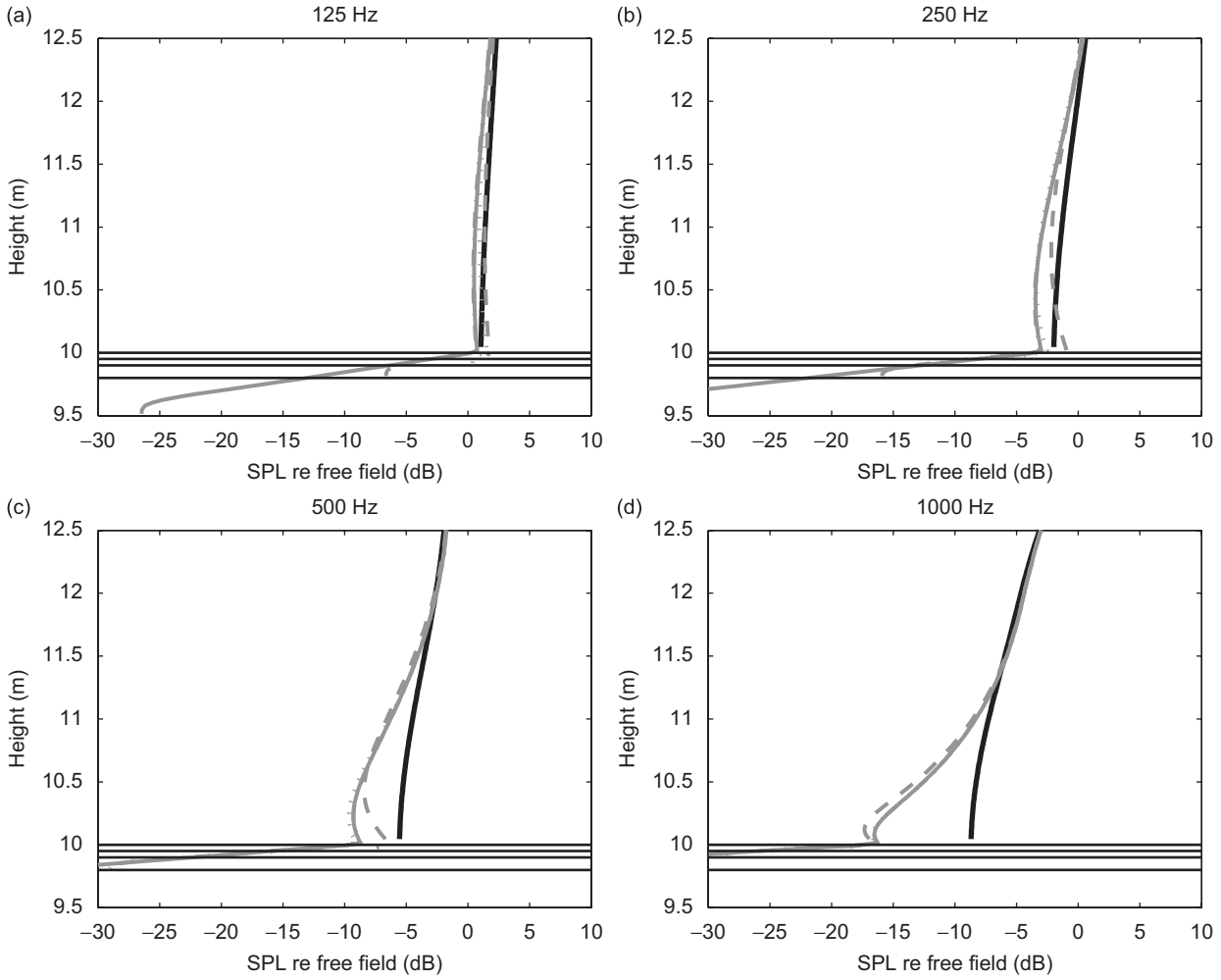

Fig. 16. Octave band sound pressure levels with centre frequencies 125 Hz (a), 250 Hz (b), 500 Hz (c), and 1000 Hz (d), relative to free field sound propagation, along a vertical line (at $x = 15$ m) above the central building. The full, black lines are for a fully rigid roof. Intensive green roofs (loose earth) with different substrate thickness are shown by the grey lines ($S = 5$ cm—full lines, 10 cm—dashed lines, 20 cm—dash-dotted lines, and 50 cm—dotted lines). The sound pressure level distributions in the soil layers are shown as well ($W_b = W_c = H = 10$ m, $D = 1$ m, coherent line source).

6. Conclusions

In this work, sound propagation over both intensive and extensive green roofs has been numerically studied using the FDTD model. The sound propagation equations in a homogeneous and still environment were considered. The building façades were modelled as fully specularly reflecting. Including the substrate layer itself in the sound propagation domain, by using the Zwikker and Kosten phenomenological ground model, allowed investigating the effect of layer thickness. The presence of plants was not considered in this study, since this mainly affects high-frequency sound, which is not important for sound propagation over high buildings. In the case of an extensive green roof, clay pellets were simulated. For the intensive green roof, a layer of loose earth was considered. Corresponding ground parameters were deduced from the literature. The spatial discretisation needed for an accurate prediction of sound reflection from the ground layers was found by means of a numerical experiment.

The influence of source type was studied in detail. The Fourier approach can be used to find an incoherent line source solution based on two-dimensional calculations. However, it cannot be straightforwardly applied

to a time-domain method, in particular for situations involving absorbing materials. Therefore, the validity of the alternative Twist method was numerically proven in a street canyon configuration by comparing it to the Fourier approach, in the case of perfectly reflecting surfaces only. In a next step, the Twist method was used to show that the effect of the presence of a green roof, relative to a rigid roof, is rather independent of source type.

In a numerical parameter study, an intensive green roof was considered, where a layer of loose earth of 40 cm was present above a 10-cm-layer of gravel. The presence of such a green roof results in an important decrease in sound pressure level at the non-exposed side of a building. This decrease is relevant when keeping in mind the quiet-side approach. In the case of an isolated building, the effect of a green roof, relative to a rigid roof, is somewhat enhanced, especially at higher frequencies. It is, however, mainly interesting to use a green roof in a street canyon configuration, since sound pressure levels at the quiet side are much higher there. The effect of the presence of a green roof, relative to a rigid one, increases with increasing octave band centre frequency, and amounts to 6 dB at 1000 Hz, when the green fraction of the roof is 0.8. This effect is very uniform over the non-exposed canyon. The width–height ratio of the street canyon has only a limited influence. There is a linear relationship between the green roof effect and the fraction of the roof covered with green, and the slopes increase with the octave band centre frequency.

Both extensive and intensive green roofs are interesting to reduce diffracting waves over a building. In the range of the typical layer thicknesses for extensive green roofs, pronounced maximum attenuations are present, depending on layer thickness and frequency. These peaks become more distinct with increasing frequency. A good overall efficiency is observed near the maximum layer thickness of extensive green roofs, which is between 15 and 20 cm. Since the substrate thickness of an intensive green roof usually exceeds 20 cm, its behaviour does not change when further increasing layer thickness. Low frequencies are hardly affected by the presence of either an extensive or intensive green roof.

Appendix A. Discretised FDTD equations

The staggered-in-space, staggered-in-time FDTD equations used for the calculations in this study are presented here. In a staggered spatial grid, the acoustic pressures are typically situated in the centre of each computational cell, the components of the particle velocity are on the faces that border each cell. The acoustic pressures are updated at the full time steps, while the particle velocities are updated at the intermediate times. This leads to the following notations in a two-dimensional simulation space: $p^{l\,\mathrm{d}t}_{(i\,\mathrm{d}x,j\,\mathrm{d}y)}$, $v^{(l+0.5)\,\mathrm{d}t}_{x((i\pm0.5)\,\mathrm{d}x,j\,\mathrm{d}y)}$, and $v^{(l+0.5)\,\mathrm{d}t}_{y(i\,\mathrm{d}x,(j\pm0.5)\,\mathrm{d}y)}$, where $\mathrm{d}x$ and $\mathrm{d}y$ are the spatial discretisation steps, and $\mathrm{d}t$ is the time-discretisation step. Indices i and j locate the spatial points, the index l the discrete times. Indices of spatial and temporal grid points are indicated as subscripts and superscripts, respectively.

The discretised FDTD sound propagation equations in free air then become:

$$v^{(l+0.5)\,\mathrm{d}t}_{x((i+0.5)\,\mathrm{d}x,j\,\mathrm{d}y)} = v^{(l-0.5)\,\mathrm{d}t}_{x((i+0.5)\,\mathrm{d}x,j\,\mathrm{d}y)} - \frac{\mathrm{d}t}{\rho_0\,\mathrm{d}x}\left(p^{l\,\mathrm{d}t}_{((i+1)\,\mathrm{d}x,j\,\mathrm{d}y)} - p^{l\,\mathrm{d}t}_{(i\,\mathrm{d}x,j\,\mathrm{d}y)}\right), \tag{A.1a}$$

$$v^{(l+0.5)\,\mathrm{d}t}_{y(i\,\mathrm{d}x,(j+0.5)\,\mathrm{d}y)} = v^{(l-0.5)\,\mathrm{d}t}_{y(i\,\mathrm{d}x,(j+0.5)\,\mathrm{d}y)} - \frac{\mathrm{d}t}{\rho_0\mathrm{d}y}\left(p^{l\,\mathrm{d}t}_{(i\,\mathrm{d}x,(j+1)\,\mathrm{d}y)} - p^{l\,\mathrm{d}t}_{(i\,\mathrm{d}x,j\,\mathrm{d}y)}\right), \tag{A.1b}$$

$$p^{(l+1)\,\mathrm{d}t}_{(i\,\mathrm{d}x,j\,\mathrm{d}y)} = p^{l\,\mathrm{d}t}_{(i\,\mathrm{d}x,j\,\mathrm{d}y)} - \rho_0 c_0^2\,\mathrm{d}t\left(\frac{v^{(l+0.5)\,\mathrm{d}t}_{x((i+0.5)\,\mathrm{d}x,j\,\mathrm{d}y)} - v^{(l+0.5)\,\mathrm{d}t}_{x((i-0.5)\,\mathrm{d}x,j\,\mathrm{d}y)}}{\mathrm{d}x} + \frac{v^{(l+0.5)\,\mathrm{d}t}_{y(i\,\mathrm{d}x,(j+0.5)\,\mathrm{d}y)} - v^{(l+0.5)\,\mathrm{d}t}_{y(i\,\mathrm{d}x,(j-0.5)\,\mathrm{d}y)}}{\mathrm{d}y}\right). \tag{A.1c}$$

The particle velocities appearing at a rigid boundary must be fixed to zero:

$$v_{x((i+0.5)\mathrm{d}x,j\,\mathrm{d}y)} = 0, \tag{A.2a}$$

$$v_{y(i\,\mathrm{d}x,(j+0.5)\,\mathrm{d}y)} = 0. \tag{A.2b}$$

The particle velocities at the façades are modelled as frequency-independent real-valued impedance planes. For a left-hand side façade, the discretised FDTD equation reads:

$$v_{x((i+0.5)\,\mathrm{d}x,j\,\mathrm{d}y)}^{(l+0.5)\,\mathrm{d}t}\left[1+\frac{\mathrm{d}tc_0Z_0}{\mathrm{d}x}\right]=v_{x((i+0.5)\,\mathrm{d}x,j\,\mathrm{d}y)}^{(l-0.5)\,\mathrm{d}t}\left[1-\frac{\mathrm{d}tc_0Z_0}{\mathrm{d}x}\right]-\frac{2\mathrm{d}t}{\rho_0\,\mathrm{d}x}p_{((i+1)\,\mathrm{d}x,j\,\mathrm{d}y)}^{l\,\mathrm{d}t}. \tag{A.3a}$$

A similar equation can be derived for a right-hand side façade:

$$v_{x((i+0.5)\,\mathrm{d}x,j\,\mathrm{d}y)}^{(l+0.5)\,\mathrm{d}t}\left[1+\frac{\mathrm{d}tc_0Z_0}{\mathrm{d}x}\right]=v_{x((i+0.5)\,\mathrm{d}x,j\,\mathrm{d}y)}^{(l-0.5)\,\mathrm{d}t}\left[1-\frac{\mathrm{d}tc_0Z_0}{\mathrm{d}x}\right]+\frac{2\mathrm{d}t}{\rho_0\mathrm{d}x}p_{(i\,\mathrm{d}x,j\,\mathrm{d}y)}^{l\,\mathrm{d}t}. \tag{A.3b}$$

In Eqs. (A.3a) and (A.3b), Z_0 is the normalised acoustic real-valued façade impedance.

The discretised equations for sound propagation in the substrate are given below:

$$v_{x((i+0.5)\,\mathrm{d}x,j\,\mathrm{d}y)}^{(l+0.5)\,\mathrm{d}t}\left[1+\frac{0.5R\mathrm{d}t\varphi}{\rho_0k_s}\right]=v_{x((i+0.5)\,\mathrm{d}x,j\,\mathrm{d}y)}^{(l-0.5)\,\mathrm{d}t}\left[1-\frac{0.5R\,\mathrm{d}t\varphi}{\rho_0k_s}\right]-\frac{\varphi\,\mathrm{d}t}{k_s\rho_0\,\mathrm{d}x}\left(p_{((i+1)\,\mathrm{d}x,j\,\mathrm{d}y)}^{l\,\mathrm{d}t}-p_{(i\,\mathrm{d}x,j\,\mathrm{d}y)}^{l\,\mathrm{d}t}\right), \tag{A.4a}$$

$$v_{y(i\,\mathrm{d}x,(j+0.5)\,\mathrm{d}y)}^{(l+0.5)\,\mathrm{d}t}\left[1+\frac{0.5R\,\mathrm{d}t\varphi}{\rho_0k_s}\right]=v_{y(i\,\mathrm{d}x,(j+0.5)\,\mathrm{d}y)}^{(l-0.5)\,\mathrm{d}t}\left[1-\frac{0.5R\,\mathrm{d}t\varphi}{\rho_0k_s}\right]-\frac{\varphi\,\mathrm{d}t}{k_s\rho_0\,\mathrm{d}y}\left(p_{(i\,\mathrm{d}x,(j+1)\,\mathrm{d}y)}^{l\,\mathrm{d}t}-p_{(i\,\mathrm{d}x,j\,\mathrm{d}y)}^{l\,\mathrm{d}t}\right), \tag{A.4b}$$

$$p_{(i\,\mathrm{d}x,j\,\mathrm{d}y)}^{(l+1)\,\mathrm{d}t}=p_{(i\,\mathrm{d}x,j\,\mathrm{d}y)}^{l\,\mathrm{d}t}-\frac{\rho_0c_0^2\,\mathrm{d}t}{\varphi}\left(\frac{v_{x((i+0.5)\,\mathrm{d}x,j\,\mathrm{d}y)}^{(l+0.5)\,\mathrm{d}t}-v_{x((i-0.5)\,\mathrm{d}x,j\,\mathrm{d}y)}^{(l+0.5)\,\mathrm{d}t}}{\mathrm{d}x}+\frac{v_{y(i\,\mathrm{d}x,(j+0.5)\,\mathrm{d}y)}^{(l+0.5)\,\mathrm{d}t}-v_{y(i\,\mathrm{d}x,(j-0.5)\,\mathrm{d}y)}^{(l+0.5)\,\mathrm{d}t}}{\mathrm{d}y}\right). \tag{A.4c}$$

References

[1] A. Niachou, K. Papakonstantinou, M. Santamouris, A. Tsangrassoulis, G. Mihalakakou, Analysis of the green roof thermal properties and investigation of its energy performance, *Energy and Buildings* 33 (2001) 719–729.

[2] H. Takebayashi, M. Moriyama, Surface heat budget on green roof and high reflection roof for mitigation of urban heat island, *Building and Environment* 42 (2007) 2971–2979.

[3] T. Theodosiou, Summer period analysis of the performance of a planted roof as a passive cooling technique, *Energy and Buildings* 35 (2003) 909–917.

[4] J. Mentens, D. Raes, M. Hermy, Green roofs as a tool for solving the rainwater runoff problem in the urbanized 21st century?, *Landscape and Urban Planning* 77 (2006) 217–226.

[5] N. Van Woert, D. Rowe, J. Andresen, C. Rugh, R. Fernandez, L. Xiao, Green roof stormwater retention: effects of roof surface, slope, and media depth, *Journal of Environmental Quality* 34 (2005) 1036–1044.

[6] E. Villarreal, L. Bengtsson, Response of a *Sedum* green-roof to individual rain events, *Ecological Engineering* 25 (2005) 1–7.

[7] H. Taha, Modeling impacts of increased urban vegetation on ozone air quality in the South Coast Air Basin, *Atmospheric Environment* 30 (1996) 3423–3430.

[8] E. Ekaterini, A. Dimitris, The contribution of a planted roof to the thermal protection of buildings in Greece, *Energy and Buildings* 27 (1998) 29–36.

[9] N. Wong, S. Tay, R. Wong, C. Ong, A. Sia, Life cycle cost analysis of rooftop gardens in Singapore, *Building and Environment* 38 (2003) 499–509.

[10] S. Schrader, M. Boening, Soil formation on green roofs and its contribution to urban biodiversity with emphasis on Collembolans, *Pedobiologia* 50 (2006) 347–356.

[11] G. Minke, G. Witter, *Haeuser mit Gruenem Pelz, Ein Handbuch zur Hausbegruenung*, Verlag Dieter Fricke GmbH, Frankfurt, 1982.

[12] E. Öhrström, Psycho-social effects of traffic noise exposure, *Journal of Sound and Vibration* 151 (1991) 513–517.

[13] T. Kihlman. Quiet side and high façade insulation—means to solve the city noise problem. *Proceedings of Internoise 2001*, The Hague, The Netherlands, 2001.

[14] T. Kihlman, M. Ögren, W. Kropp, Prediction of urban traffic noise in shielded courtyards, *Proceedings of Internoise 2002*, Dearborn, MI, USA.

[15] M. Ögren, W. Kropp, Road traffic noise propagation between two dimensional city canyons using an equivalent sources approach, *Acta Acustica United with Acustica* 90 (2004) 293–300.

[16] T. Van Renterghem, *The Finite-Difference Time-Domain Method for the Simulation of Sound Propagation in a Moving Medium*, Ph.D. Thesis, Universiteit Gent, Belgium, 2003.

[17] T. Van Renterghem, E. Salomons, D. Botteldooren, Parameter study of sound propagation between city canyons with coupled FDTD-PE model, *Applied Acoustics* 67 (2006) 487–510.

[18] D. Heimann, Three-dimensional linearised Euler model simulations of sound propagation in idealised urban situations with wind effects, *Applied Acoustics* 68 (2007) 217–237.
[19] T. Van Renterghem, E. Salomons, D. Botteldooren, Efficient FDTD-PE model for sound propagation in situations with complex obstacles and wind profiles, *Acta Acustica United with Acustica* 91 (2005) 671–679.
[20] J. Defrance, E. Salomons, I. Noordhoek, D. Heimann, B. Plovsing, G. Watts, H. Jonasson, X. Zhang, E. Premat, I. Schmich, F. Aballea, M. Baulac, F. de Roo, Outdoor sound propagation reference model developed in the European Harmonoise project, *Acta Acustica United with Acustica* 93 (2007) 213–227.
[21] D. Botteldooren, Finite-difference time-domain simulation of low-frequency room acoustic problems, *Journal of the Acoustical Society of America* 98 (1995) 3302–3308.
[22] C. Zwikker, C. Kosten, *Sound Absorbing Materials*, Elsevier, New York, 1949.
[23] E. Salomons, R. Blumrich, D. Heimann, Eulerian time-domain model for sound propagation over a finite-impedance ground surface. Comparison with frequencydomain models, *Acta Acustica United with Acustica* 88 (2002) 483–492.
[24] K. Heutschi, M. Horvath, J. Hofmann, Simulation of ground impedance in finite difference time domain calculations of outdoor sound propagation, *Acta Acustica United with Acustica* 91 (2005) 35–40.
[25] K. Wilson, V. Ostashev, S. Collier, N. Symons, D. Aldridge, D. Marlin, Time-domain calculations of sound interactions with outdoor ground surfaces, *Applied Acoustics* 68 (2007) 173–200.
[26] K. Wilson, V. Ostashev, S. Collier, Time-domain equations for sound propagation in rigid-frame porous media, *Journal of the Acoustical Society of America* 116 (2004) 1889–1892.
[27] K. Attenborough, Ground parameter information for propagation modeling, *Journal of the Acoustical Society of America* 92 (1992) 418–427.
[28] O. Umnova, K. Attenborough, H. Shin, A. Cummings, Response of multiple rigid porous layers to high levels of continuous acoustic excitation, *Journal of the Acoustical Society of America* 116 (2004) 703–712.
[29] D. Duhamel, Efficient calculation of the three-dimensional sound pressure field around a noise barrier, *Journal of Sound and Vibration* 197 (1996) 547–571.
[30] P. Jean, J. Defrance, Y. Gabillet, The importance of source type on the assessment of noise barriers, *Journal of Sound and Vibration* 226 (1999) 201–216.
[31] M. Hornikx, J. Forssén, The 2.5-dimensional equivalent sources method for directly exposed and shielded urban canyons, *Journal of the Acoustical Society of America* 122 (2007) 2532–2541.
[32] E. Salomons, A. Geerlings, Comparison of a ray model and a Fourier-boundary element method for traffic noise situations with multiple diffractions and reflections, *Acta Acustica United with Acustica* 83 (1997) 35–47.